System Identification of Dynamic Systems With Cubic Nonlinearities Using Linear Time-Periodic Approximations

Article · January 2009

DOI: 10.1115/DETC2009-87364

CITATIONS
8

READS
933

2 authors:

Mathew S. Allen
Brigham Young University - Provo Main Campus
221 PUBLICATIONS **2,897** CITATIONS

SEE PROFILE

Michael W. Sracic
University of Wisconsin–Madison
28 PUBLICATIONS **379** CITATIONS

SEE PROFILE

Proceedings of the ASME 2009 International Design Engineering Technical Conferences & Computers and Information in Engineering Conference
IDETC/CIE 2009
Aug. 30-Sept. 2, 2009, San Diego, California, USA

DETC2009-87364

SYSTEM IDENTIFICATION OF DYNAMIC SYSTEMS WITH CUBIC NONLINEARITIES USING LINEAR TIME-PERIODIC APPROXIMATIONS

Matthew S. Allen* &
Assistant Professor
Michael W. Sracic
Graduate Research Assistant

Department of Engineering Physics
University of Wisconsin-Madison
*msallen@engr.wisc.edu

ABSTRACT

This work develops methods to identify parametric models of nonlinear dynamic systems from response measurements using tools for Linear Time Periodic (LTP) systems. The basic approach is to drive the system periodically in a stable limit cycle and then measure deviations of the response from that limit cycle. Under certain conditions, the resulting response can be well approximated as that of a linear-time periodic system. In the analytical realm it is common to linearize a system about a periodic trajectory and then use Floquet analysis to assess the stability of the limit cycle. This work is concerned with the inverse problem, using a measured time-periodic response to derive a nonlinear dynamic model for the system. Recently, a few new methods were developed that facilitate the experimental identification of linear time periodic systems, and those methods are exploited in this work. The proposed system identification methodology is evaluated by applying it to a Duffing oscillator, demonstrating that the nonlinear force-displacement relationship can be identified without a priori knowledge of its functional form. The proposed methods are also applied to simulated measurements from a cantilever beam with a cubic nonlinear spring on its tip, revealing that the model order of the system and the displacement dependent stiffness can be readily identified.

1. INTRODUCTION

While a wealth of tools are available today that can be used to model, design, and test linear dynamic systems, nonlinear systems pose a much greater challenge. Many systems can be well approximated as linear within a certain range of a measurable quantity such as displacement. For example, stress and energy theory describing beams is well approximated as linear when the beam is thin and long and deflections of the beam are very small with respect to its other dimensions. But even an ideal beam will begin to behave nonlinearly beyond some threshold of response. In fact, virtually all real systems behave nonlinearly if their inputs are large enough. There is increasing interest in nonlinear dynamic phenomena in automotive, aerospace [1-3], micro [4, 5] and biological systems [6].

Despite significant effort, experimental methods for characterizing nonlinear dynamic system are still quite limited. Kerschen et al. present an excellent review of nonlinear system identification methods [7], as do Adams and Allemang [8]. All available methods are currently limited to relatively low order systems, and all but a few methods require one to assume a form for the nonlinearity a priori. It can be very difficult to experimentally assess the order of the nonlinear system and to assure that the a priori form assumed for the nonlinearities is appropriate.

A suite of tools was recently developed by the authors that allows one to identify the parameters of linear time-periodic (LTP) systems experimentally [9] . A few other methods also exist [10-14]. The methods developed by the authors are the LTP analog to experimental modal analysis, allowing one to identify the order of the system from experimental measurements and identifying a parametric model for the system using robust, well established tools for linear time-invariant (LTI) systems. Allen simulated system identification of a Jeffcott rotor on anisotropic bearings and then demonstrated how the state transition matrix and dynamic system matrix can be reconstructed from the experimentally

identified parametric model. These methods have been applied to continuous-scan laser-Doppler vibrometer measurements, verifying their applicability to a relatively high order, complicated nonlinear dynamic system [15, 16]. This work applies these new LTP identification methods to identify the parameters of two nonlinear systems having cubic nonlinearities. The systems are excited in a stable, periodic limit cycle and then perturbed from that limit cycle slightly. Assuming that the system is well approximated as LTP with respect to that limit cycle, the LTP identification methods can then be applied to identify a model for the system. That model is then used together with the measured steady-state limit cycle to develop a model for the nonlinear system.

The following section describes the proposed nonlinear system identification technique and reviews some of the important concepts involved in the LTP identification methods presented in [9]. A more complete development of the theory can be found in [9, 16-19] . Section 3 presents two analytical models that are used to generate simulated measurements. The proposed techniques are evaluated by applying them to these simulated measurements. The first model is a single degree of freedom Duffing Oscillator and the second is an Euler-Bernoulli cantilever beam with a cubic nonlinear spring at its tip, modeled using a two-term Ritz series.

2. THEORY

A broad range of systems can be described in the general form given in Equation 1, where *x* is the state of the system, *t* is a time variable, *u* is the input applied to the system and y is the response or output of the system. Both the functions *f* and *h* are nonlinear.

$$\begin{aligned} \dot{x}(t) &= f(t, u(t), x(t)) \\ y(t) &= h(t, u(t), x(t)) \end{aligned} \tag{1}$$

Many important nonlinear systems exhibit purely or nearly purely periodic motion, such as a helicopter rotor rotating at a constant rate or a human walking periodically. When the motion can be accurately described as periodic with period T_A $\bar{x}(t+T_A)=\bar{x}(t)$, then the nonlinear system can be linearized about that periodic trajectory resulting in linear time periodic model that is valid for small perturbations $\tilde{x}(t)=x(t)-\bar{x}(t)$ about the periodic trajectory, $\bar{x}(t)$ [17]. Under certain conditions, the nonlinear dynamic model for the system can be approximated using a Taylor Series expansion of the function *f* about the periodic trajectory,

$$f(u,x) = f(\bar{u},\bar{x}) + \frac{\partial f(\bar{u},\bar{x})}{\partial x}(x-\bar{x}) + \frac{\partial f(\bar{u},\bar{x})}{\partial u}(u-\bar{u}) + \cdots \tag{2}$$

where it is understood that $\bar{x}(t)$ and $\bar{u}(t)$ are functions of time. A similar result follows from expanding *h* in a Taylor Series. The system model then becomes the following,

$$\begin{aligned} \dot{\tilde{x}}(t) &= A(t)\tilde{x}(t) + B(t)\tilde{u}(t) \\ \tilde{y}(t) &= C(t)\tilde{x}(t) + D(t)\tilde{u}(t) \end{aligned} \tag{3}$$

where the time periodic matrices are as follows, with *i* and *j* denoting the elements in the i^{th} row and j^{th} column of the matrices for i=1,2,..,N and j=1,2,..,N and where N is the number of states.

$$\begin{aligned} A(t)_{ij} &= \left[\frac{\partial f_i}{\partial x_j}\right]_{x=\bar{x}(t),u=\bar{u}(t)}, \; B(t)_{ij} = \left[\frac{\partial f_i}{\partial u_j}\right]_{x=\bar{x}(t),u=\bar{u}(t)}, \\ C(t)_{ij} &= \left[\frac{\partial h_i}{\partial x_j}\right]_{x=\bar{x}(t),u=\bar{u}(t)}, \; D(t)_{ij} = \left[\frac{\partial h_i}{\partial u_j}\right]_{x=\bar{x}(t),u=\bar{u}(t)} \end{aligned} \tag{4}$$

Equation 3 constitutes a set of linear time-periodic state space equations which govern the dynamics of the system about the periodic trajectory, $\bar{x}(t)$. This work focuses on the case where the only input applied is $\bar{u}(t)$, which keeps the system in a periodic orbit, so $\tilde{u}(t)=0$. The response about the periodic trajectory, $\tilde{x}(t)$, can then be described using the State Transition Matrix (STM) $\Phi(t,t_0)$.

$$x(t) = \Phi(t,t_0)x(t_0) \tag{5}$$

Floquet theory allows one to decompose the fundamental matrix as the product of a periodic vector of Floquet mode shapes $\Psi(t)=[\phi_1(t), \phi_2(t), \ldots]$ and a diagonal matrix of Floquet Exponents Λ [18-20].

$$\Phi(t,t_k) = \Psi(t)\exp\left(\Lambda(t-t_k)\right)\Psi(t_k)^{-1} \tag{6}$$

Allen developed two methods for identifying $\Psi(t)$ and Λ from experimental measurements [9], dubbed the Fourier Series Expansion technique (FSE) and the Lifting technique.

2.1. Fourier Series Expansion Technique (FSE)

The STM representation in Equation 6 can be written in summation form as follows:

$$\begin{aligned} \Phi(t,t_k) &= \sum_{r=1}^{N} \left(R(t)\right)_r \exp\left(\lambda_r\left(t-t_k\right)\right) \\ \left(R(t)\right)_r &= \left\{\phi_r(t)\right\}\left\{M_r(t_k)\right\}^T \end{aligned} \tag{7}$$

where $(R(t))_r$ is the r^{th} residue matrix corresponding to the rth Floquet exponent λ_r, $\phi_r(t)$ is the r^{th} periodic mode shape and column of $\Psi(t)$, $M_r(t_k)$ is the r^{th} column of $[\Psi(t_k)]^{-T}$. Because the mode shapes are periodic, the residue matrices $(R(t))_r$ are also periodic and can be expanded in a Fourier Series resulting in the following,

$$\Phi(t,t_k)=\sum_{r=1}^{N}\sum_{m=-N_B}^{N_B}[B]_{r,m}\exp\left(\left(\lambda_r+im\omega_A\right)\left(t-t_k\right)\right) \quad (8)$$

where a complete description requires $N_B = \infty$, but the periodic residue can often be well approximated with finite N_B. The fundamental frequency of the LTP system is $\omega_A=2\pi/T_A$. Equation 8 is equivalent to the free response of an LTI system with order $2N(2N_B+1)$. Each mode gives rise to exponential terms in the STM with exponents $\lambda_r+im\omega_A$, however, these eigenvalues are just the positive and negative harmonics (sidebands) of the r^{th} Floquet exponent.

2.2. Lifting Technique

An alternative technique was also developed based on "lifting" the response [21]. If one samples an integer number of times, P, per fundamental period, then one can construct P responses,

$$y_k(n)=y\left(t_k+nT_A\right) \quad (9)$$

for $k = 1\ldots P$ and where n ranges over the length of the signal. Each response $y_k(n)$ contains a set of time samples that are P samples apart, and since one is always sampling at the same point within the fundamental period, the periodic eigenvectors of the STM appears to be constant. One can then collect the k responses into a lifted response vector whose size is P times the number of outputs and use standard LTI system identification methods to identify a parametric model for the system. An attractive feature of this method is that the responses in Equation 9 retain the some order as the original system response, so they are relatively easy to interrogate. The parametric model obtained from the lifted responses can be transformed into a continuous FSE model and used to reconstruct the STM and time-varying state matrix, $A(t)$, of the system [16].

3. SIMULATED EXPERIMENTS

The following sections describe the models of the Duffing Oscillator (DO) and the Cantilever Beam modeled with a low-order Ritz series (CRB). Simulated responses are generated and the proposed methods are applied. The identified system model is then compared with the known analytical model to assess the techniques.

3.1. Duffing Oscillator

Figure 1 illustrates a single degree-of-freedom model of a Duffing Oscillator where x is the displacement degree of freedom, m is the system mass, c is a damping coefficient, k_{nl} is nonlinear spring stiffness, and f_d is an excitation force. The nonlinearity comes from a spring constant that is dependent on the displacement of the mass as well as on the cube of the displacement.

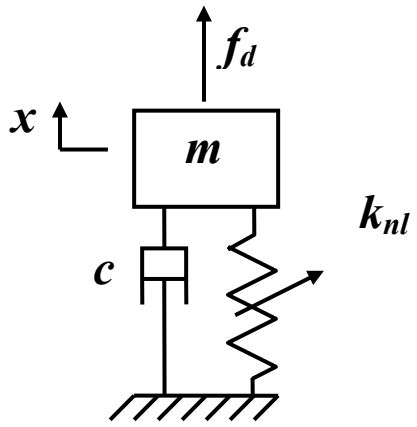

Figure 1: Single degree-of-freedom oscillator with a nonlinear spring.

The restoring spring force is equal to:

$$F_{sp}=k_1x+k_3x^3 \quad (10)$$

and the spring stiffness is therefore a function of x.

$$k_{nl}(x)=k_1+k_3x^2 \quad (11)$$

The equation of motion for this system is nondimensionalized by dividing all terms by the mass and defining nondimensional time so that the natural frequency is unity resulting in the following,

$$\ddot{x}+2\zeta\omega_1\dot{x}+\omega_1x=f-\omega_3x^3 \quad (12)$$

where f is the nondimensional force $f=f_d/m$. When excited with a harmonic force, this system exhibits steady state periodic motion after the transients have dissipated. The parameters used in this study are: ζ=0.02, ω_1=1 and ω_3=0.5. The system is driven with the following nonlinear, periodic forcing function.

$$f_{ext}(t) = \left(\omega_1^2 - \Omega^2\right) A \sin(\Omega t) + \cdots$$
$$\Omega \frac{c}{m} A \cos(\Omega t) + \frac{k_3}{m} A^3 \sin^3(\Omega t) + f_{impulse}(t) \quad (13)$$

This complicated excitation signal was chosen because it produces a purely sinusoidal with amplitude A, making the example and subsequent discussion somewhat clearer. In practice one would not know how to excite a system to produce such a response, so one would probably just excite the system with a sinusoid as is done in Section 3.2.

$$x(t) = A \sin(\Omega t). \quad (14)$$

The parameters used here are A=1 and Ω=0.9. An impulsive force $f_{impulse}$ is also included which represents a disturbance that is used to drive the system away from this periodic limit cycle. The response of the system as it returns to the periodic limit cycle is approximated by an LTP system and its parameters are identified.

3.1.1. Duffing Oscillator Simulation Results

Equations 12 and 13 are used to simulate the nonlinear response of the Duffing Oscillator system using MATLAB's adaptive Runge-Kutta (ode45) time integration routine. The first integration was used to find the limit cycle response. The solution was evaluated with a sampling frequency of approximately f_{samp}=6.37 Hz, which results in 22 samples per cycle of the harmonic response. A second integration was then performed with an impulsive force applied on top of the harmonic forcing to perturb the system from its steady state trajectory. A half-sine was used for the impulsive force,

$$f_{impulse}(t) = A_{impulse} \frac{2\bar{\tau}}{\pi} \sin\left(\frac{\pi}{\bar{\tau}} t\right) \quad (15)$$

where $A_{impulse}$ is the amplitude of the pulse and $\bar{\tau}$ is the duration of the impulse, with $A_{impulse}$=5000 and $\bar{\tau}$=0.01. Both the impulse response and the limit cycle response were evaluated for a time window length containing 184 full cycles of the harmonic response frequency. This allowed sufficient time for the impulse response to decay until only the steady state signal remained. Figure 2 shows the time responses of the steady state and steady state plus the perturbation signals. The top pane contains both of these response signals plotted on top of each other. The lower pane contains the signal that results from subtracting off the steady state portion of the perturbed plus steady state signal.

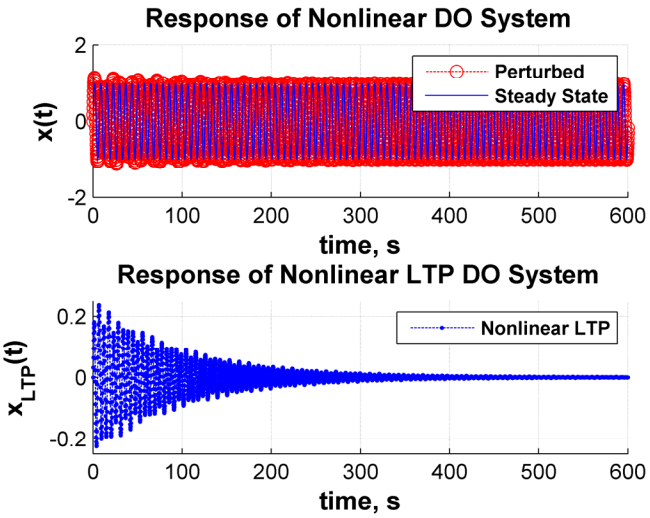

Figure 2: (top) Full response of nonlinear DO excited by the superposition of harmonic and impulse excitation. (bottom) Resulting LTP response after linearizing the nonlinear response about the periodic trajectory.

Figure 3 contains the spectrums of the responses. The blue curve corresponds to the FFT of the nonlinear response and the dashed red curve is the spectrum of the LTP response.

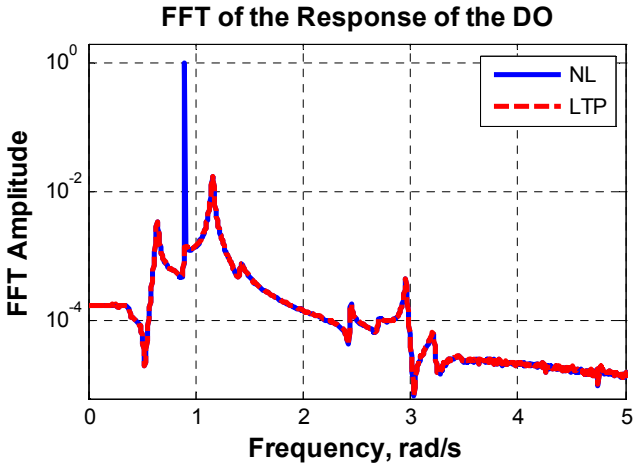

Figure 3: Frequency spectrums of the responses of the DO. The red dashed curve corresponds to the full nonlinear simulation. The dashed red curve is the frequency spectrum of the LTP signal from the impulse response of the DO linearized about the periodic trajectory.

The spectrum of the nonlinear response in blue contains one sharp peak at the frequency of the steady state response. There are also a few other broader peaks near 0.64, 1.16, and 2.24, and 2.96 rad/s. These peaks all occur at 1.16 rad/s plus or minus integer multiples of the drive frequency (negative frequencies are reflected back onto positive ones). In light of Equation 8, one can surmise that the system has only one degree of freedom but is significantly time-periodic.

Next we apply the lifting technique to the LTP response, producing 22 pseudo-LTI responses. Figure 4 below shows a composite FRF (or average of the magnitude) of the 22 pseudo-responses (gray solid line). The composite FRF contains one strong peak at 0.26 rad/s, revealing that there is only one strongly excited mode in this LTP response. The Algorithm of Mode Isolation (AMI) [22-24] was used to identify the modal parameters of the lifted response. The green dotted curve corresponds to the reconstruction of the composite FRF based on the parameters that were identified by AMI. The red dashed curve corresponds to the difference between the measured data and the reconstruction, revealing that the one-mode reconstruction parameterizes the response very well. AMI identified an eigenvalue of 0.2589 rad/s and a damping ratio of 0.0378 for the LTP system.

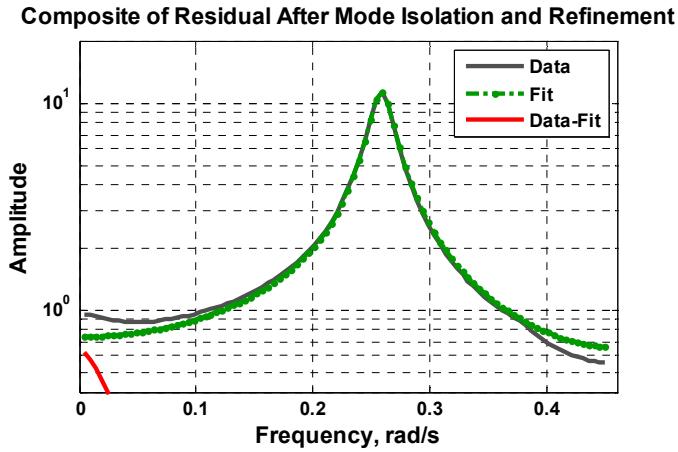

Figure 4: (gray) Composite FRF of 22 pseudo-reponses resulting from applying the lifting method to the LTP DO response. (green dotted) Reconstructed composite FRF identified by AMI. (red dashed) Composite FRF of the difference between the measurement (gray) and the reconstruction (red).

Here we have conveniently measured the state of the DO, so the LTP model can now be used to reconstruct the STM of the system from the identified parametric model for the displacement and the derivative of that model, as was done in [15, 16, 25, 26]. The STM was fully determined after just one cycle, and therefore the limit cycle of the system is stable. Once the STM has been constructed over one cycle, the time varying $A(t)$ matrix can be found from the STM and its derivative. This gives the instantaneous stiffness and damping of the system at each point within the fundamental cycle. The fundamental cycle was also measured (the steady state response) and used with the identified $A(t)$ matrix to plot the force-displacement curve for the system. The result is shown in Figure 5. The Stochastic Subspace system identification routine [26] was also applied to the LTP response in the time domain, and the reconstruction of the force-displacement curve based on the parameters identified by SSI is also shown. An analytical model of the nonlinear system linearized about this periodic trajectory was also created and its response simulated and identified, and the corresponding description of the force displacement curve is also shown (Fit LTP).

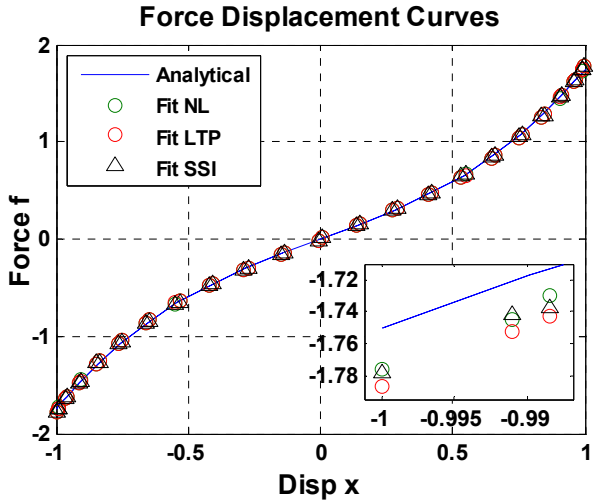

Figure 5: Force Displacement Curves for the Duffing Oscillator System. The blue line corresponds to the known analytical force-displacement function used to simulation the motion. Markers are shown for the reconstructed force-displacement curve found by applying the identification to the simulated nonlinear response (Fit NL), to the same using the Subspace System Identification (SSI) routine, and to a simulated purely LTP response (Fit LTP).

3.1.2. Discussion of the Duffing Oscillator Results

The blue line spectrum in Figure 3 shows significant evidence of nonlinearity in the system because it contains only one harmonic of the forcing function. Recall that the harmonic forcing function in Equation 13 (excluding the impulse force), which contains three harmonics, excited a system response that contained only one harmonic. After subtracting off the steady-state response, the resulting spectrum shows clear evidence of time periodicity. The strong peak at 1.16 rad/s is the main harmonic of the mode of this spectrum; or the zero harmonic in the FSE of the mode. If the system were linear then only this peak would occur. The peak at 0.64 rad/s just to the left of the zero harmonic is a second harmonic term which would appear at 1.16 rad/s – 2*0.9 rad/s = -0.64 rad/s, but it folds back to +0.64 rad/s. The peak at 2.96 rad/s is the second harmonic of the mode at 1.16 rad/s + 2*0.9 rad/s = 2.96 rad/s. The peak at 2.44 rad/s can be deciphered be the conjugate of the fourth harmonic, and one can continue in this fashion to visually interpret the other notable peaks in the spectrum. These sidebands occur according to Equation 8 and illustrate that the system is behaving linearly about the periodic limit cycle. If the system was purely linear, one would expect the zero harmonic frequency content to occur at the linear natural frequency of 1 rad/s instead of at 1.16 rad/s, but for a time-periodic system the response peaks at the Floquet exponent, which is not equal to the natural frequency of the linearized system.

The spectrums that result from applying the lifting technique to the LTP signal are much simpler to interpret and appear to be of the same order as the original signal. The composite spectrum, which is the gray curve in Figure 4 contains one strong peak which AMI identified at a frequency of 0.2589 rad/s, corresponding to an alias of the Floquet exponent. Aliasing occurs because the lifting technique resamples the measurement, changing the effective bandwidth of the signals, but it is of little consequence because the aliased Floquet exponent provides a perfectly valid description of the LTP system. The eigenvalue identified by AMI corresponds to the zero harmonic peak at 1.16 rad/s in the FSE representation of Figure 3. Both the Lifting and FSE techniques give similar results for this system, although the Lifting technique is somewhat simpler to apply.

3.2. Cantilever Ritz Beam with Nonlinear Spring

The second system considered for this work is a cantilever beam with a cubic nonlinear spring attached to the tip and is shown in Figure 6. The coordinate, x, describes the location along the axis of the beam, v describes the transverse deflection at a given position x, and f describes an external forcing function applied to the beam's free end. The beam is assumed to have uniform parameters: densityρ, elastic modulus E, cross sectional area A, and length L.

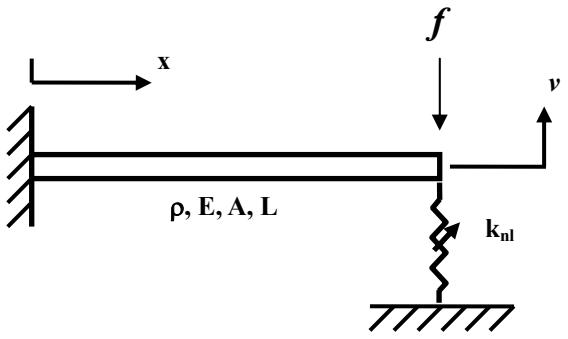

Figure 6: Continuous cantilever beam system with a nonlinear spring attached to the tip.

This system can be achieved in experiment [7] and therefore makes for an interesting simulation because one can control the geometric nonlinearity of the tip spring. A Ritz Series representation was used to create a finite-order model for the beam. Assuming a uniform, prismatic beam that behaves linear-elastic, mode shapes corresponding to transverse bending motion can be used as shape functions to construct an efficient Ritz Series representation [27]. The transformation takes the form,

$$v(x,t)=\sum_{r=1}^{N}\psi_r(x)q_r(t) \tag{16}$$

where $\psi_r(x)$ is the r^{th} Euler-Bernoulli beam mode shape for a cantilever, $q_r(t)$ is the r^{th} generalized coordinate, and N is the number of modes used. The system's undamped equations of motion are provided in Equation 17 in generalized transverse displacement coordinates.

$$\rho AL[M]\ddot{q}+\frac{EI}{L^3}[K]q=Q=\sum f_{ext}\psi_r(x_f) \tag{17}$$

The generalized force vector Q is a sum of the product between all external forces and the value of the shape function at the application of the force. Q also contains the nonlinear spring force. As with the single degree of freedom DO, it is convenient to divide the equation by the leading coefficients, and then nondimensionalize the system to have a first natural frequency equal to unity. This can be done with the following change of variables in the equations of motion

$$\tau=\omega_1 t,\quad \frac{\partial\tau}{\partial t}=\omega_1 \tag{18}$$

where τ is the nondimensional time variable, ω_1 is the first natural frequency of the system, and $\bar{q}$ is the generalized coordinate with respect to nondimensional time. After utilizing the chain rule of differentiation, the first and second time derivatives of the generalized coordinates with respect to nondimensional time become

$$\dot{q}=\omega_1\dot{\bar{q}},\quad \ddot{q}=\omega_1^2\ddot{\bar{q}}. \tag{19}$$

If the substitutions are made, the equations of motion take the following form,

$$\begin{gathered}[M_{nd}]\ddot{\bar{q}}+[C_{nd}]\dot{\bar{q}}+[K_{nd}]\bar{q}=Q_{nd}\\ [M_{nd}]=[M],\quad [K_{nd}]=\frac{1}{\alpha_1^4}[K],\quad Q_{nd}=\frac{3}{\alpha_1^4 k_{static}}Q\\ [C_{nd}]=[M_{nd}][\phi_{nd}][diag(2\zeta_r\omega_r)][\phi_{nd}]^T[M_{nd}]\\ \alpha_1^4=\omega_1^2\frac{\rho AL^4}{EI},\quad k_{static}=\frac{3EI}{L^3}\end{gathered} \tag{20}$$

where modal damping has been added to the equation based on performing an eigenvector analysis on the nondimensional mass and stiffness matrices, and $[\phi_{nd}]$ is a matrix containing the eigenvectors in the columns. The parameters α_1^4 and k_{static} were defined in terms of the beams physical parameters to simplify the notation. The parameters used for the simulation were ω_1=1, α_1=1.8751 [27], and k_{static}=3. Two modes were used in

the Ritz Series and the second natural frequency was ω_2=6.27 rad/s. Modal damping at ζ=0.01 was applied to each of the modes and two total modes were used in the simulation. The generalized force term Q includes Ritz series formulated contributions from any external force on the tip (shown as f in Figure 6) as well as the restoring force due to the spring [27]. The beam provides linear stiffness at the tip due to its flexural rigidity, so the nonlinear spring stiffness is chosen to be purely nonlinear as given below.

$$k_{nl} = k_3 v_{tip}^2 \tag{21}$$

The physical restoring force due to the spring is then equal to

$$f_{sp} = k_3 v_{tip}^3 \tag{22}$$

The nonlinear spring constant was given a value k_3=3. In Equations 21 and 22, v_{tip} is the transverse displacement of the beam at the tip in physical coordinates. The external force included contributions of a harmonic forcing function given by Equation 23 and an impulsive force which was approximated by a half-sine as in Equation 24.

$$f_{ss}(t) = F_{ss} \sin(\Omega t) \tag{23}$$

$$f_i(t) = F_i \sin\left(\frac{\pi}{\bar{\tau}}\left(t - T_p\right)\right) \tag{24}$$

In Equation 24, $\bar{\tau}$ is the pulse duration and T_p is the time at which the pulse is initiated.

3.2.1. Cantilever Ritz Beam Results

The equations of motion of the CRB were formed in state space and solved using time-integration. In the simulation, the force amplitudes were F_{ss}=12 and F_i=9 and the time parameters were: Ω=6, $\bar{\tau}$ =0.05, and T_p=2.111e+3. The frequency of the excitation was chosen to excite the beam near its second linearized natural frequency. The system exhibited a purely periodic response after all of the transients had dissipated. After the system reached this steady state trajectory, the impulse was applied to perturb the response away from its limit cycle slightly. The response was then recorded for 672 cycles of the drive frequency, Ω. This allowed for the transient vibration to decay completely, leaving only the steady state response once again. Figure 7 shows steady state and perturbed time responses. The top pane contains both of these response signals plotted on top of each other. The lower pane contains the signal that results from subtracting the steady state response from the perturbed response.

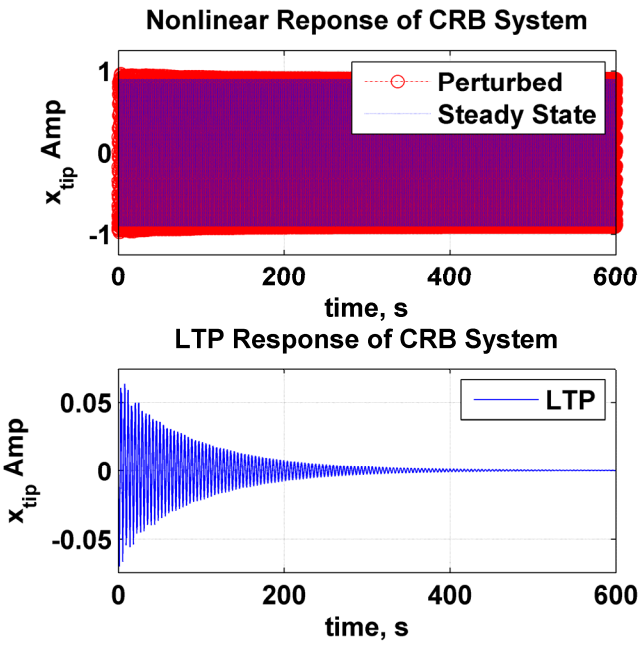

Figure 7: (top) Full response of nonlinear CRB excited harmonically and with an impulse superimposed on the harmonic force. (bottom) Difference of the two responses in the upper pane. This response can be approximated as LTP under the assumptions in Section 2.

The FFT of the nonlinear and LTP responses was computed and the resulting spectra are shown in Figure 8. The spectrum of the nonlinear CRB response (dashed blue) contains two sharp peaks occurring at 6 and 18 rad/s, corresponding to the steady state response of the beam at the drive frequency and one of its harmonics. These are absent from the LTP response indicating that the steady state response has been effectively removed. Both the nonlinear and LTP spectra contain two broader peaks at 1.5 and 6.4 rad/s. These peaks have the familiar shape associated with linear modes and occur near the structure's low-amplitude, linear natural frequencies, which are 1 and 6.27 rad/s. According to the theory presented previously, each of the peaks in the LTP spectra are expected to occur at the Floquet exponents of the system. The fact that the first peak occurs at 1.5 rad/s, significantly higher than the first linear natural frequency, suggests that the system is time-periodic so that its Floquet exponents are not equal to its linear eigenvalues. Furthermore, the two other peaks near 10.5 rad/s and 13.5 rad/s can be interpreted as harmonics of the Floquet exponent at 1.5 rad/s, and provide evidence that this response is that of an LTP system and hence that the underlying system is nonlinear. Specifically, one can attribute the peak at 13.5 rad/s can be attributed to the second harmonic of the Floquet exponent at 1.5 rad/s, and the peak at 10.5 rad/s to the second harmonic of the conjugate exponent at -1.475 rad/s (-1.475 rad/s+2*6 rad/s = 10.525).

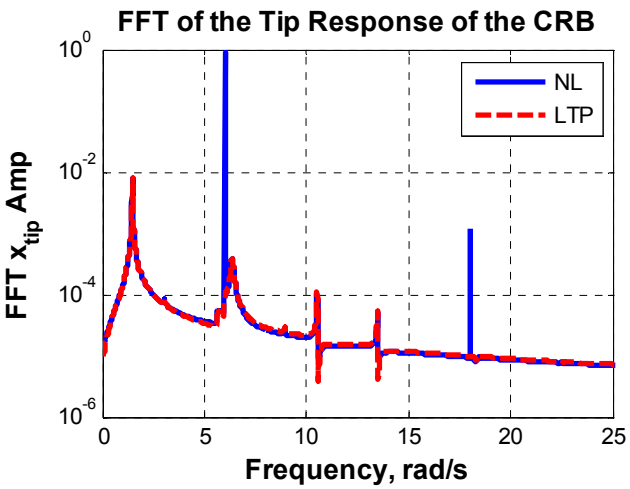

Figure 8: Frequency spectrums of the responses of the CRB. The red dashed curve corresponds to the full nonlinear simulation. The dashed red curve is the frequency spectrum of the LTP signal from the impulse response of the CRB linearized about the periodic trajectory.

The lifting method was applied to the LTP response of the beam resulting in 32 pseudo-responses because the sampling frequency was precisely 32 times higher than the harmonic forcing frequency. Figure 9 shows a composite FRF of the frequency spectra of the lifted pseudo-responses (in gray), the reconstruction of the composite FRF based on the parameters identified from AMI, and a composite of the difference between the two. Two peaks occur near 0.35 rad/s and 1.5 rad/s, so the system appears to be second order. AMI identified two eigenvalues from the set of lifted FRFs, corresponding frequencies of 0.3664 rad/s (λ= -0.0629+i0.3609) and 1.4730 rad/s (λ= -0.0100+i1.4730) rad/s. Although the limit cycle stability of the CRB was not studied in this work, the fact that the real parts of the eigenvalues of the LTP response are negative is evidence to suggest that the limit cycle of the CRB is stable. As noted previously with the DO, the lifted signals alias the true frequencies; one could obtain an equally valid LTP model with these same Floquet exponents after adding any integer multiple of the fundamental frequency to the imaginary part of each. The unaliased frequencies can be deciphered again using Equation 8 as an aid. The strongest peak is at a frequency that is less than the bandwidth of the lifted signal, and a strong peak exists at the same frequency in Figure 8. The eigenvalue identified at 0.3664 rad/s could be associated with the peak at 6.4 rad/s in the FSE spectra if one adds 6 to the imaginary part of that eigenvalue.

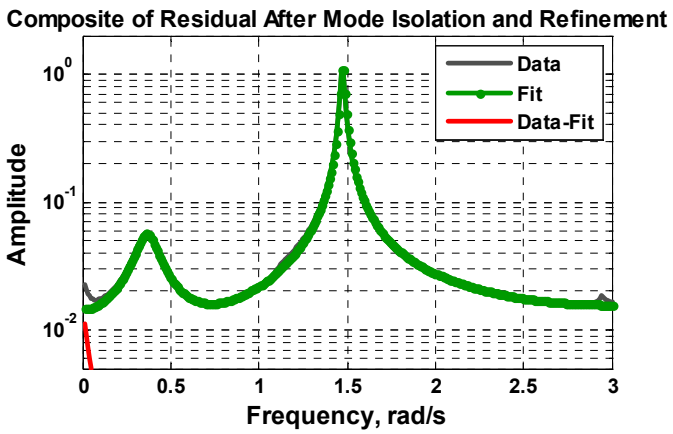

Figure 9: (gray) Composite FRF of 32 pseudo-responses obtained by lifting the LTP response of the cantilever beam. (green dotted) Reconstructed composite FRF identified by AMI. (red dashed) Composite FRF of the difference between the measurement (gray) and the reconstruction (red).

The parameters identified from the lifted responses were used to reconstruct the STM for the LTP system and then the time varying State Matrix $A(t)$ over one period. The FFT of the residues found by the lifting method gives the FSE coefficients $B_{r,m}$, which are shown in Figure 10. All 32 identified terms are shown with blue circles. As discussed in [9], it was necessary to truncate the higher order terms in the FSE, because small errors in these terms would be amplified when computing the derivative of the STM. The seven largest coefficients were kept and are highlighted with red dots. The values of the coefficients that were retained were $B_{1,m}$ =1.45e-6, 1.47e-4, 2.18e-5, 4.09e-3, 8.79e-7, 3.16e-05, and 1.68e-6 for m= -4, -2, -1, 0, 1, 2, and 4 respectively.

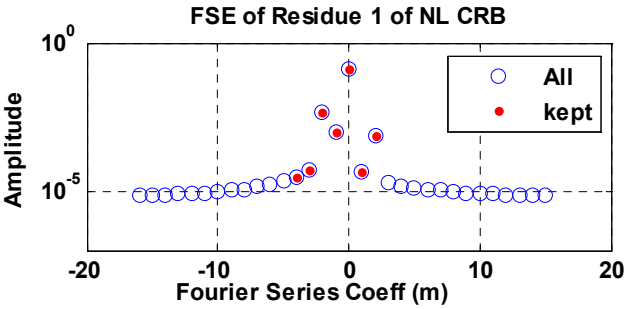

Figure 10: Fourier coefficient magnitudes of the FSE of the first LTP residue of the NL CRB. The open blue circles are all the coefficients for the residue. The red dots correspond to the significant coefficients that were kept for the expansion.

Having obtained the modal parameters of the state transition matrix, the STM can now be constructed for one period [9, 15, 16, 25]. However, the measurement set contains 10 outputs yet the system is only second order. To overcome this, two of the measurement locations were chosen to be the states of the system (one at the mid-span of the beam and one at the tip). The STM was then computed for these states. Singular-value

decomposition was applied to the time-periodic eigenvectors in order to verify that only two states were needed to reconstruct the response of the system at any of the others. The time varying $A(t)$ matrix can also be estimated from the fundamental cycle of the CRB response. Since the fundamental cycle was also measured, the estimated $A(t)$ coefficient terms of $A(t)$ can be plotted versus tip displacement. An analytical model for the $A(t)$ matrix was also produced from the numerical integration. Figure 11 shows the two terms from a partition of the $A(t)$ matrix which corresponds to $-M^{-1}K$ calculation, and so they are related to the stiffness of the system. The analytical coefficients(blue line) and estimated (black dotted line) $A(t)$ stiffness coefficient results are both provided.

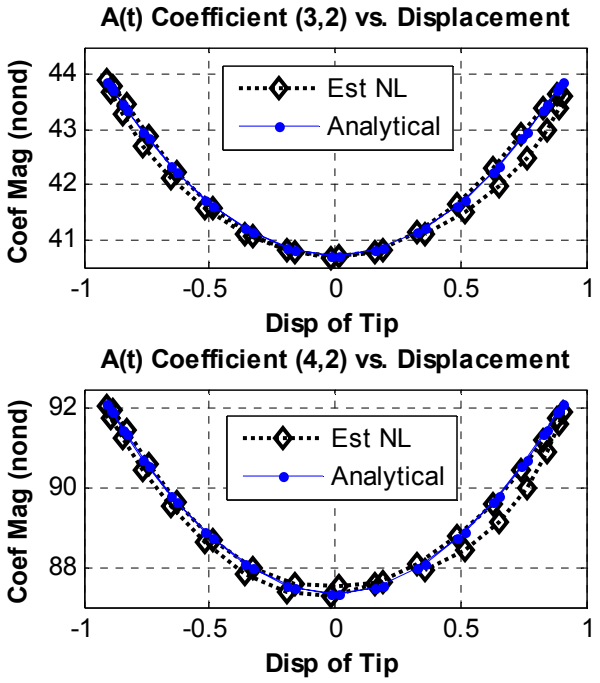

Figure 11: Displacement varying terms from the estimated and analytical A(t) matrix plotted versus tip displacement of the CRB.

3.2.2. Discussion of the Cantilever Ritz Beam Results

The CRB system was clearly behaving nonlinearly, as evidenced by the fact that the steady-state response contained a component at the forcing frequency 6 rad/s and its third harmonic (18 rad/s in Figure 8). In this work we have ignored that information and applied LTP identification to the system because it lends itself to straightforward interpretation and because existing tools for LTI systems can be used to perform parameter identification. In the future, the steady-state response should also be used in the identification process in order to make use of all available information.

Both the FSE and lifting methods were applied to identify a parametric model of the LTP system. Both contain the same information, but as noted in [15, 16], the lifted spectra are significantly easier to interpret and standard LTI system identification routines such as AMI can be applied directly to the lifted spectra to identify the LTP model, whereas one must use a somewhat modified approach to treat the full spectrum in Figure 8. However, the FSE of the identified residual matrices can be used to retain only the useful information for estimating the STM and $A(t)$ matrix, so it seems that one would be wise to consider both the FSE and lifted representations when identifying the parameters of a system.

4. CONCLUSIONS

This paper presented a method for using Linear Time Periodic system identification techniques to identify the parameters of a nonlinear system excited in a stable, periodic limit cycle. Two analytical models containing cubic nonlinearities were used to test the methods: a single degree of freedom Duffing Oscillator (DO) and a two degree of freedom cantilever beam (CRB) that was modeled using the Ritz method. The systems were driven such that they oscillated in stable limit cycles and their response for small perturbations about each limit cycle was shown to be well approximated as linear time periodic. A linear time-periodic model was identified from the measurements and was used to construct the nonlinear model for the system.

. The focus of this work was not on the stability of the limit cycles for the systems. The DO was found to have a stable limit cycle by numerical integration and construction of the STM from a single cycle. The stability of the CRB was assumed here. Future works will consider the overall stability of the established limit cycle for the CRB as well as look at the sensitivities of the DO and CRB limit cycles to changes in the design variables.

The LTP responses obtained for both systems were interrogated and clear evidence of time-periodicity was observed, illustrating the relative ease with which the LTP spectra can be understood. After using the lifting method, a standard modal parameter identification algorithm for LTI systems was used to identify the modal parameters of the LTP systems, correctly identifying the model order of the system in each case. The methods in [16, 25] were used to reconstruct the state transition matrix and time varying system matrix $A(t)$ for the DO. The time varying state matrix of the DO was then used to reconstruct the restoring force relationship of the DO, and this was compared with the analytical restoring force and shown to agree quite well. A similar analysis was pursued for the CRB showing that both the order of the system and a few of its time-periodic parameters could be identified from the responses. Components from the time varying state matrix of the CRB was used to display the displacement dependent coefficient terms of the $A(t)$ matrix of the CRB, and this was compared with the analytical coefficients and shown to agree quite well.

The methods and results presented are significant because the entire identifications were performed without assuming an a priori form for the restoring force of the DO or for the order

and functional form of the nonlinearity for the CRB. The only assumption was that the limit cycle was stable and that the response could be approximated as LTP about that limit cycle. These preliminary results suggest that the proposed nonlinear identification methods may facilitate identification of relatively high order systems with complicated nonlinearities. One strength of the proposed method is that one can use familiar tools such as frequency spectra and LTI identification routines to interrogate the measurements and extract the system model.

5. REFERENCES

[1] P. S. Beran, N. S. Khot, F. E. Eastep, R. D. Snyder, and J. V. Zweber, "Numerical analysis of store-induced limit-cycle oscillation," *Journal of Aircraft,* vol. 41, pp. 1315-1326, 2004.

[2] N. J. Lindsley, C. L. Pettit, and P. S. Beran, "Nonlinear plate aeroelastic response with uncertain stiffness and boundary conditions," *Structure and Infrastructure Engineering,* vol. 2, pp. 201-20, 2006.

[3] A. H. Nayfeh, M. R. Hajj, S. A. Nayfeh, C. C. Chabalko, and P. S. Beran, "A Reduced-Order Model for LCO Dependence on Mach Number in F16 Flight Tests," in *49th AIAA/ASME/ASCE/AHS/ASC Structures, Structural Dynamics, and Materials Conference* Schaumburg, IL, 2008.

[4] M. Allen, H. Sumali, and D. Epp, "Piecewise-linear restoring force surfaces for semi-nonparametric identification of nonlinear systems," *Nonlinear Dynamics,* vol. 54, pp. 123-135, 2008.

[5] J. F. Rhoads, S. W. Shaw, K. L. Turner, J. Moehlis, B. E. DeMartini, and Z. Wenhua, "Generalized parametric resonance in electrostatically actuated microelectromechanical oscillators," *Journal of Sound and Vibration,* vol. 296, pp. 797-829, 2006.

[6] J. B. Dingwell and J. P. Cusumano, "Nonlinear time series analysis of normal and pathological human walking," *Chaos,* vol. 10, pp. 848-63, 2000.

[7] G. Kerschen, K. Worden, A. Vakakis, and J. Golinval, "Past, Present and Future of Nonlinear System Identification in Structural Dynamics," *Mechanical Systems and Signal Processing,* vol. 20, pp. 505-592, 2006.

[8] D. E. Adams and R. J. Allemang, "Survey of Nonlinear Detection and Identification Techniques for Experimental Vibrations," in *International Seminar on Modal Analysis (ISMA 23)* Leuven, Belgium, 1998, pp. 269–281.

[9] M. S. Allen, "Frequency-Domain Identification of Linear Time-Periodic Systems using LTI Techniques," *Journal of Computational and Nonlinear Dynamics,* vol. Accepted, 2009.

[10] N. M. Wereley and S. R. Hall, "Linear time periodic systems: transfer functions, poles, transmission zeroes and directional properties," in *Proceedings of the 1991 American Control Conference* Boston, MA, USA: American Autom. Control Council, 1991, pp. 1179-84.

[11] J. J. Hench, "A technique for the identification of linear periodic state-space models," *International Journal of Control,* vol. 62, pp. 289-301, 1995.

[12] S. Hwang, "Frequency Domain System Identification of Helicoptor Rotor Dynamics Incorporating Models with Time Periodic Coefficients," in *Department of Aerospace Engineering*. vol. Doctor of Philosophy: University of Maryland - College Park, 1997.

[13] A. Siddiqui, "Identification of the Harmonic Transfer Functions of a Helicopter Rotor," in *Department of Aeronautics and Astronautics*. vol. M.S.: Massachusetts Institute of Technology, 1999, p. 88.

[14] S. Sang Joon, C. E. S. Cesnik, and S. R. Hall, "System identification technique for active helicopter rotors," *Journal of Intelligent Material Systems and Structures,* vol. 16, pp. 1025-38, 2005.

[15] M. S. Allen and M. W. Sracic, "Mass normalized mode shapes using impact excitation and continuous-scan laser Doppler vibrometry," in *Italian Association of Laser Velocimitry and non-Invasive Diagnostics (AIVELA)* Ancona, Italy, 2008.

[16] M. S. Allen and M. W. Sracic, "A Method for Generating Pseudo Single-Point FRFs from Continuous Scan Laser Vibrometer Measurements," in *26th International Modal Analysis Conference (IMAC XXVI)*, Orlando, Florida, 2008.

[17] C. Chen, *Linear Systems Theory and Design*, 3 ed. New York: Oxford University Press, Inc., 1999.

[18] G. Floquet, "Sur Les Equations Lineairs a Coefficients Periodiques," *Ann. Sci. Ecole Norm. Sup.,* vol. 12, pp. 47-88, 1883.

[19] L. A. Luxemburg, "Frequency Analysis ofTime-Varying Periodic Linear Systems by Using Modulo p Transforms and Its Applications to the Computer-Aided Analysis of Switched Networks," *Circuits, Systems, and Signal Processesing,* vol. 9, pp. 3-29, 1990.

[20] H. D'Angelo, *Linear time-varying systems: analysis and synthesis*. Boston: Allyn and Bacon, 1970.

[21] P. Arambel and G. Tadmor, "Robust H_{oo} Identification of Linear Periodic Discrete-Time Systems," *International Journal of Robust and Nonlinear Controol,* vol. 4, pp. 595-612, 1994.

[22] M. S. Allen and J. H. Ginsberg, "A linear least-squares version of the algorithm of mode isolation for identifying modal properties. Part I: Conceptual Development," *Journal of the Acoustical Society of America (JASA),* vol. 116, pp. 900-907, 2004.

[23] M. S. Allen and J. H. Ginsberg, "A linear least-squares version of the algorithm of mode isolation for identifying modal properties. Part II: Application and Assessment," *Journal of the Acoustical Society of America (JASA),* vol. 116, 2004.

[24] M. S. Allen and J. H. Ginsberg, "A Global, Single-Input-Multi-Output (SIMO) Implementation of The Algorithm of Mode Isolation and Applications to Analytical and Experimental Data," *Mechanical Systems and Signal Processing,* vol. 20, pp. 1090–1111, 2006.

[25] M. Allen and J. H. Ginsberg, "Floquet Modal Analysis to Detect Cracks in a Rotating Shaft on Anisotropic Supports," in *24th International Modal Analysis Conference (IMAC XXIV)*, St. Louis, MO, 2006.

[26] P. Van Overschee and B. De Moor, *Subspace Identification for Linear Systems: Theory-Implementation-Applications*. Boston: Kluwer Academic Publishers, 1996.

[27] J. H. Ginsberg, *Mechanical and Structural Vibrations Theory and Applications*, 1 ed. New York: John Wiley & Sons, Inc., 2001.